Graphene-Based Ceramic Nanocomposites

Subjects: Nanoscience & Nanotechnology

Contributor: Nestor Washington Solis Pinargote, Anton Smirnov

In the present work, the state of the art of the most common additive manufacturing (AM) technologies used for the manufacturing of complex shape structures of graphene-based ceramic nanocomposites, ceramic and graphene-based parts is explained. The most important works about the fabrication of composites using graphene-based ceramic pastes by Direct Ink Writing (DIW) are disclosed in detail and illustrated with representative examples. Various examples of the most relevant approaches for the manufacturing of graphene-based ceramic nanocomposites by DIW are provided. Furthermore, different feedstock formulations and their corresponding rheological behavior were explained.

Keywords: additive manufacturing ; graphene oxide ; graphene-based paste ; Direct Ink Writing ; ceramic nanocomposites

1. Introduction

A ceramic is a nonmetallic, inorganic solid[1], which has exceptional and diverse physical and chemical properties that characterize it as a multipurpose material. Typical properties that can be found in ceramics materials are ultra-high-temperature ability, excellent wear resistance, great hardness and mechanical strength, high melting points, good thermal stability, and chemical inertness, low density, and low electrical and thermal conductivity. Thanks to these properties, ceramics are used in multifunctional applications such as biomedical engineering, electronics, aerospace, chemical industry, and machinery[2]. Note that the advantage of ceramics over other materials is the ability to obtain predetermined characteristics by changing the raw materials composition and the production technology[3][4][5][6][7][8]. Commonly, raw materials are composed by mixtures of ceramic powders with or without binders and additives, and these mixtures are used to form green bodies with desired simple shape by different forming methods as dry pressing, slip casting, injection molding, gel casting, tape casting, extrusion and others[9][10]. After forming, the green parts are very soft; therefore, it is necessary to apply heat upon them to get a dense product by sintering. Sintering can be defined as a thermal process at higher temperatures with or without pressure for compacting and forming a solid structure via mass transport events that often occur on the diffusional processes[10]. Although traditional methods of ceramic forming are well-studied and widespread, they have several drawbacks such as high cost, long processing times and the impossibility of producing pieces with interconnected holes or with highly complex shapes. In addition, for obtaining a sintered ceramic part with high surface quality and accuracy, mechanical post-processing work is necessary. This post-process work is expensive and time-consuming due to the natural high hardness and brittleness of ceramics materials[2][11].

Over the past 30 years, new technologies for processing materials called additive manufacturing (AM) have been developed rapidly and they are being introduced more and more every day in a wide range of fields thanks to their ability to produce, in a very fast and cheap way, complex 3d parts by adding material instead of cutting it away. AM, also known as three-dimensional (3D) printing technologies[12], can be explained as a technique of blending materials by either fusion, binding, or solidifying materials such as liquid resin and different powders materials. These technologies build a part in a precisely adding material layer-by-layer fashion using 3D computer-aided design (CAD) modeling[13], and their advantages include design freedom, low-quantity economy, material efficiency, reduced assembly and predictable production.

AM involves a group of advanced manufacturing technologies that allow the flexible production of precise structures with highly complex shapes, which are complicated to manufacture using conventional methods like machining or casting[14].

In 2015, the International Organization for Standardization Technical Committee (ISO/TC 261) on AM together with the American Society for Testing Materials (ASTM) Committee F42 released a new International Standard ISO/ASTM 52900:2015 in which the terms used in AM are established and defined[15]. In this standard, the AM technologies have been classified into groups taking into consideration the feedstock type, the deposition technique, and the fusing or solidification way of material. Table 1 categorizes the most popular AM technologies in the industry today into the following groups: vat photopolymerization, material jetting, binder jetting, powder bed fusion, direct energy deposition, sheet lamination, and material extrusion.

Table 1. Groups of additive manufacturing technologies by the International Organization for Standardization (ISO)/American Society for Testing Materials (ASTM) 52900:2015.

Category	Additive Manufacturing Technology Type	Abbreviation	Feedstock
Vat photopolymerization	Stereolithography	SLA	Liquid photopolymers, hybrid polymer-ceramic, hybrid polymer-graphene
	Digital Light Processing	DLP	
	Two-Photon Polymerization	TPP	
	Continuous Liquid Interface Production	CLIP	Liquid photopolymers
Powder bed fusion	Multi Jet Fusion	MJF	Thermoplastic polymers
	Selective Laser Sintering	SLS	Plastics, composites
	Selective Laser Melting	SLM	Metals
	Electron Beam Melting	EBM	Metals
Material jetting	Material Jetting	MJ	Photopolymers
	NanoParticle Jetting	NPJ	Metals, ceramics
	Drop On Demand	DOD	Wax, ceramic-, graphene-inks
Material Extrusion	Fused Deposition Modeling	FDM	Thermoplastic polymers, metal-, ceramic-, graphene-reinforced polymers
	Direct Ink Writing	DIW	Ceramics
Direct Energy Deposition	Electron Beam Additive Manufacturing	EBAM	Metals and alloys in the form of powder or wire
	Laser Engineering Net Shape	LENS	
Binder jetting	Binder Jetting	BJ	Ceramic, metal, gypsum, sand
Sheet Lamination	Laminated Object Manufacturing	LOM	Ceramic, metal-filled tapes, paper, polymer composites.

The main differences between each of the categories mentioned above can be summarized as follows[16]:

- In vat photopolymerization the 3D object is created layer by layer thanks to the curing of a liquid photopolymer resin under the influence of an ultraviolet (UV) light. The liquid photopolymer is held in a vat with a built support submerged near the surface of the resin. Then the UV light is directed to the resin surface following a determined path thus allowing a selective local polymerization of the liquid photopolymer. After that, the built support is re-submerged into the resin and the process is repeated until the 3D object is fully obtained;

- The material jetting principle is used to create a solid 3D object layer by layer from droplets, which are mainly composed of liquid photopolymer resin, that are selectively sprayed by an inkjet-style printhead and immediately cured thanks to the expose of a UV light. Commonly, technologies that work under this principle are compared to the two-dimensional (2D) inkjet printing, which deposits only a single layer of ink droplets;

- In the technologies that operate under the principles of binder jetting a liquid binder, which is selectively deposited by drops onto a powder-based material using an inkjet-style print head, is utilized in order to produce a solid 3D object layer by layer. During the process, alternate layers of powder material and binding material are depositing as follow: powder particles are spread over a built support using a roller while the print head deposits the liquid binder, which acts as a glue between powder particles and layers, on top of the powder bed; after that, the built support is lowered by the model's layer thickness and then the process is repeated until the 3D object is formed;

- The powder bed fusion category utilizes an energy source that allows the local sintering or melting between the particles of a powder material for the forming of a solid 3D object layer by layer. The energy sources can be lasers or electron beams depending on the using material powder. The electron beam is necessary for metals, while lasers are required for polymers. The forming part process is very similar to binder jetting: powder particles are spread over a built support using a roller while the energy source fuses the first layer; after that, the built support is lowered by the model's

layer thickness and a new layer of powder is spread across the previous layer repeating the process until the 3D object is formed;

- In direct energy deposition the 3D object is created layer by layer thanks to the directly melting of build-material and deposing them on the workpiece using a focused thermal energy source such as laser, electron beam or plasma arc. This principle can be applied for a wide kind of materials such as polymers, ceramics, and metal framework composites; however, it is predominantly used for wire and powder metals, which explains why this technology is often called metal deposition. Direct energy deposition utilizes a nozzle mounted on a multi-axis arm can move freely in any direction of the x, y and z-axes that deposits melted material onto the predetermined workpiece surface, where it is automatically solidified;

- In sheet lamination a 3D part is created by bonding together, layer-by-layer, thin sheets of material (usually supplied via a system of feed rollers), which is then cutting into a final 3D object. In the process, the sheet material is positioned on the cutting bed and then it is bonded over the previous layer using any suitable sticky method; after that, the required shape is cut by laser or knife and the process is repeated until the 3D object is formed. Laminated object manufacturing (LOM) and ultrasonic consolidation (UC) are both examples of sheet lamination techniques;

- Material extrusion is a category of AM, in which the 3D object is formed by a layer by layer selective deposition of the extruded build-material through a nozzle in a continuous stream. In material extrusion, the layers are built when the nozzle deposits a viscoelastic material where it is required. The following layers are added on top of previous layers and bonded upon deposition as the material shows viscoelastic behavior. In the last past years, this technology became popular in the world for its use in 3D printers. Direct Ink Writing (DIW) and Fused deposition modeling (FDM) are the two common technologies that operate under the principles of material extrusion. However, in the last past years, a new AM technique named Pyro-EHD Tethered Electrospinning (TPES) that is based on electrohydrodynamic processes and can be related to material extrusion category became more and more popular[17][18][19].

The introduction of AM into the ceramic forming process proposes a powerful way of producing complex 3D parts. However, despite the wide variety of AM technologies, only a few of them can be implemented for printing ceramic parts. Among such technologies, the so-called Direct Ink Writing (DIW) offer greater versatility and particular suitability for the fabrication of ceramic parts[20]. DIW, also referred to as Robocasting[21], is an extrusion-based technique used in 3D printing in which new materials can be implemented most economically and flexibly[22][23]. The main requirement of this technology is the use of pastes with controlled rheological behavior that allows them to be able to be extruded into filaments capable of maintaining their shape and not collapsing during the 3D object forming process[24]. The required rheological characteristics can be achieved through the correct selection of the number of components, solid-phase parameters and the additives used[25].

In the industrial manufacture of ceramic parts, it is very common the use of slurry that contains various additives, such as plasticizers, dispersants, surfactants, binders, defoamers, lubricants, etc., which in many occasions produce the formation of defects during sintering[26]. These defects can be related to the evaporation of the aforementioned additives that leads to volumetric shrinkage and crack formation, which considerably reduces the mechanical properties of the part[27].

Some years ago, the use of chemically modified graphene (in other words, graphene oxide (GO)) has been proposed with aim of prepare an aqueous paste without any additive for the 3D printing of graphene-based heaters[28]. Later, García-Tunñoón et al. formulated free additives pastes of diverse materials, based only on the use of GO as a dispersant, rheological modifier, and binder[29]. It was possible, because GO has a great similarity to clay, including its viscoelastic behavior. Clay has exceptional chemistry and structure that permit the design of water-based suspensions for shaping with excellent viscoelastic behavior in a procedure that cannot be done with any other natural material[30]. The special combination of surface chemistry and the structure of GO sheets in contact with water under special conditions allow the preparation of a very stable GO suspension with viscoelastic behavior comparable to clay[29][31]. In addition, GO as an oxide can be homogeneously dispersed in water, and, consequently, mixtures of graphene oxide with any ceramic oxide can be processed following conventional ceramic processing routes[32][33][34][35]. Therefore, the implementation of GO to obtain ceramic pastes without additives for their use in AM opens up new possibilities for obtaining complex parts with the help of robocasting technology.

2. Direct Ink Writing Technology of Graphene-Based Ceramic Pastes

DIW is among the most commonly used AM technique for the production of 3D parts from a graphene-based paste. For obtaining a part with good properties by DIW a high graphene content paste and with a suitable raw material is necessary[36]. Besides, a high colloid volume fraction in the paste will minimize the drying-induced shrinkage after printing.

Very often, the use of additives (binders, viscosifiers, among others) is needed to provide a good dispersion of the graphene-based materials and obtain a paste with appropriate viscoelastic properties. In DIW, the paste viscosity for printing, which is related to the loss (i.e., viscous) modulus (G″), should be in the order of 10^3–10^6 mPa·s, which are very high values. On the other hand, the storage (i.e., elastic) modulus (G′) is associated with the paste elastic property thus, high values of G′ are required, because the higher G′ the stiffer is the paste with a solid-like response[37]. The yield stress and storage modulus G′ will be restored during ink exit from the nozzle, i.e., will remain their shape and dimension.

In the state of the art of graphene-based/ceramic 3D printed composites by DIW, diverse works with different applications as conductive ceramic nanocomposites[38][39], energy storage/conversion systems, high-temperature filters, and others, can be found.

Roman-Manso et al. first reported the study of 3D architected graphene/ceramic composites obtained by DIW. These composites are applied in energy storage/conversion systems, high-temperature filters, or as catalyst supports, gas sensors, and acoustic metamaterials. These 3D objects were printed starting from a paste containing homogeneous mixtures of SiC ceramic powders and up to 20 vol% of graphene nanoplatelets (GNPs), and then, these objects were consolidated by Spark Plasma Sintering (SPS), Figure 1 [38]. The paste was prepared as follows: three powder compositions were formulated with diverse GNPs contents (5, 10 and 20 vol%). The ceramic powder was mainly composed of b-SiC and using Al_2O_3 and add Y_2O_3 as sintering aids, and holding the SiC:Al_2O_3:Y_2O_3 formulation constant at a 93:2:5 (wt%) ratio for all the compositions. To obtain a homogeneous powder composition, the aforementioned components were mixed in an attrition mill with alumina balls in an isopropyl alcohol media. At the same time, a stable dispersion of GNPs in isopropanol was prepared by sonication. Next, the ceramic composite and the GNPs dispersion were mixed and, finally, stirred and sonicated. Subsequently, the solvent was removed in a rotary evaporator, and the mixture was dried at 120 °C and sieved through a 63 µm mesh. With aim of preparing the pastes, well-dispersed suspensions of the as-obtained dried blend in an aqueous polymer solution of polyethylenimine (PEI), methylcellulose (MC) and ammonium polyacrylate (APA) were obtained in a planetary centrifugal mixer. In these suspensions, PEI, MC, and APA acted as a dispersant, viscosifying agent and flocculant, respectively. The aqueous polymer composition for pastes with contents up to 10 vol%. of GNPs was (4 wt% of PEI, 5 wt% of MC and 0.3 wt% of APA); while the paste with 20 vol%. a slightly higher of the PEI concentration (5 wt%) to obtain the required pseudoplastic properties. Note that the solids concentrations in the pastes were in the range of 69–71 wt% (42–44 vol%) in all cases. Next, 3D architected composites were manufactured using a DIW printer. After printing, the parts were heated up to 415 °C to burn out the organics and, then, the as-printed parts were sintered in an SPS furnace at 1800 °C and an Argon atmosphere. Sintered composites showed high porosity, ranging from 1.6 to 0.9 g/cm^3 for corresponding GNPs contents of 0 to 20 vol%, as compared with theoretical values of the bulk compositions 3.28 g/cm^3 and 3.03 g/cm^3 for the monolithic SiC and for the 20 vol% GNPs composites, respectively. Besides, the electrical conductivity of the scaffolds demonstrates some anisotropy with the architecture character and grows with the GNPs volume fraction. It was stated that, under such an approach, the values of up to 611 and 273 S/m for the longitudinal and transverse orientations, respectively, of the structures relative to the extruded cylinders were obtained. This anisotropy was determined by the design of the structure and also by the strong preferential orientation of the GNP within the rod during the printing process.

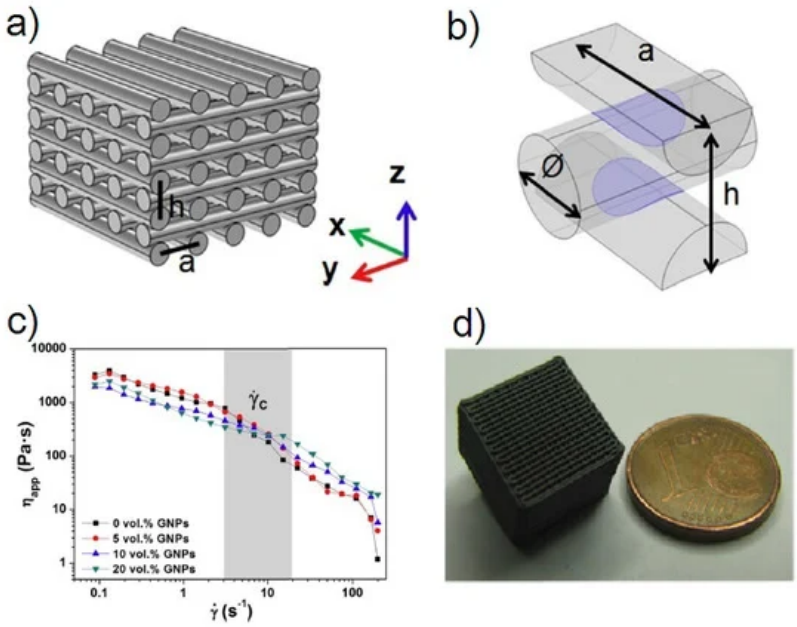

Figure 1. (**a**) Patterned structure used for scaffolds designing and (**b**) scheme of the contact area between two orthogonal rods, where *h*, *a*, and *Ø* correspond to the distance between two equivalent layers in the z direction, the distance between two adjacent rods, and the rod diameter, respectively. (**c**) Apparent viscosity as a function of the shear rate for the GNPs/SiC pastes formulated with 0, 5, 10 and 20 vol% GNPs in the powder compositions. (**d**) View of a 10 vol% GNPs/SiC sintered scaffold. Reproduced from[38], with permission from Elsevier, 2016.

Tubio et al. proposed a scalable fabrication of rGO/Al_2O_3 composites with complex mesoscale architecture by DIW for their use in diverse applications[40]. The paste production involved three basic steps: dispersion, mixing, and gelation. In the first step, an aqueous Al_2O_3 colloidal suspension with diverse graphene oxide concentration (0.5, 1 and 5 wt%) was prepared in a planetary mixer. Then, the concentration of the as as-prepared suspension was increased by water evaporation at room temperature and mixed again several times. Subsequently, hydroxypropyl methylcellulose (HPMC) was added to increase the viscosity followed by other mixed steps. Next, polyethylenimine (PEI) was added to facilitate the gelation followed by other mixed steps. The rheological tests under steady and dynamic shear conditions were carried out to investigate the printability of as-prepared pastes. The data results showed two important effects: all pastes have shear-thinning (i.e., pseudoplastic) behavior, and the GO concentration influence on the viscosity data in the studied shear-rate range. Moreover, the highest apparent viscosity was found in the paste with graphene oxide concentration of 5 wt% and this paste showed a storage modulus (G′) ~1 × 10^6 Pa, while the shear yield stress raised to 220 Pa from 20 Pa for paste with 0 wt% GO. Therefore, paste with 5 wt% GO content was used for the fabrication of GO/Al_2O_3 composites with complex mesoscale architecture by DIW. The rGO-Al_2O_3 composites were sintered in a protective atmosphere (N_2) at 1600 °C. In another work, Moyano et al. proposed a new formulation of graphene-based pastes for producing self-supported 3D architectures by DIW. Here, the authors showed that is possible to obtain graphene-based pastes from just a single surfactant to achieve a suitable high elastic modulus and a shear-thinning behavior at rest. At the same time, the whole paste produce process is simple and scalable. Three aqueous graphene-based pastes were created by mixing GO, GNP and their mixture (GNP (92.7 wt%) and GO (7.3 wt%)) with an aqueous solution (30 wt% concentration) of Poloxamer 407, a triblock copolymer that contains 70 wt% of PEO units. Pastes with 30 wt% solution of Poloxamer 407 display shear thinning characteristics. The G′ values of the three inks were 8 × 10^5 Pa, 4 × 10^5 Pa and 3 × 10^5 Pa for GNP, GO and their mix, respectively, Figure 2b [41]. These storage moduli values are larger compared with those reported for equivalent water-based GNP and GO inks, which were prepared by utilizing polyelectrolytes (anionic and cationic)[42]. The yield stress, which is related to the change of the inks to a semi-liquid state, stays between 1 and 4 kPa. Subsequently, the as-prepared pastes were used for the printing of 3D structures. Next, the structures achieved a very high compressive strength (above 2 MPa) after thermally treated at 1200 °C with a low density (0.12 g/cm^3) and very high electrical conductivity (above 4 × 10^3 S/m) for the mix GO–GNP composition.

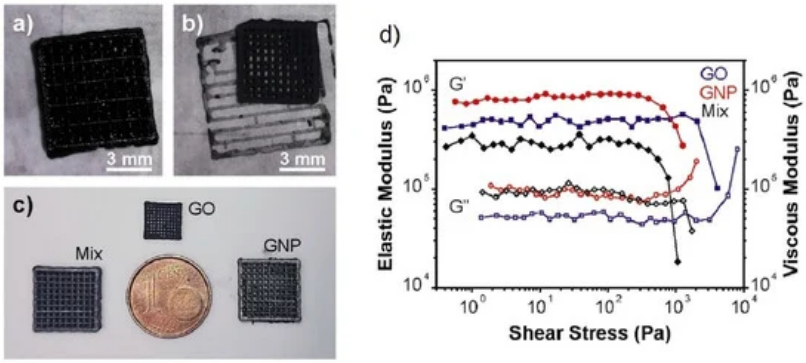

Figure 2. (**a**) 3D printed GO structure, (**b**) “a” dried 24 h in air; (**c**) Comparison of structures obtained after treatment at 1200 °C from GNP, GO and mix compositions; (**d**) Storage (G′) and loss (G″) moduli versus shear stress for the three inks: GO, GNP and mix. Reproduced from[41], with permission from Elsevier, 2019.

The previous examples showed that the classic production of graphene-based ceramic pastes involves the use of various polymers, which are later removed to get a composite of both ceramic and graphene-based materials. Different works have been carried out to develop new formulations and methods of paste preparation to reduce the number of additives in them.

One solution can be to modify the paste rheological behavior to reach suitable viscoelastic characteristics by adding some amount of silica. For example, Zhu et al. investigated the method for manufacturing 3D graphene composite aerogel with periodic macropores for supercapacitor by DIW, Figure 3 [43]. Here, to prepare a suitable paste for DIW the GO suspension (40 mg/mL) was mixed with hydrophilic fumed silica. Silica acted as a viscosifier that imparted both shear-thinning behavior and a shear yield stress to the GO suspension to enhance the printability of the GO-based paste.

Besides, the authors added several graphene nanoplatelets (GNPs) along with a reactant (resorcinol–formaldehyde (R–F) solution) to induce gelation post-printing via organic sol-gel chemistry. GNPs and SiO_2 concentrations ranged from 0 to 16.7 wt% for both materials. The results demonstrated that the apparent viscosity of as-prepared composite paste (GO–GNP) shows orders of magnitude higher than that of the GO suspension; moreover, both of them were shear-thinning non-Newtonian fluids. The presence of the GNP and silica fillers in the pure graphene oxide ink has led to improved storage modulus and yield stress more than one order of magnitude. The magnitudes of these main rheological characteristics coincide with those stated for other colloidal inks fabricated for DIW. In order to obtain the 3D graphene aerogel (GA) the printed composite was subjected to gelation, freeze-drying or supercritical-drying, and etching of the silica with hydrofluoric acid. Although in this work efforts were made to avoid the addition of polymer additives, the inclusion of silica did not completely solve this problem, since a reactant was still used for gelation of the paste.

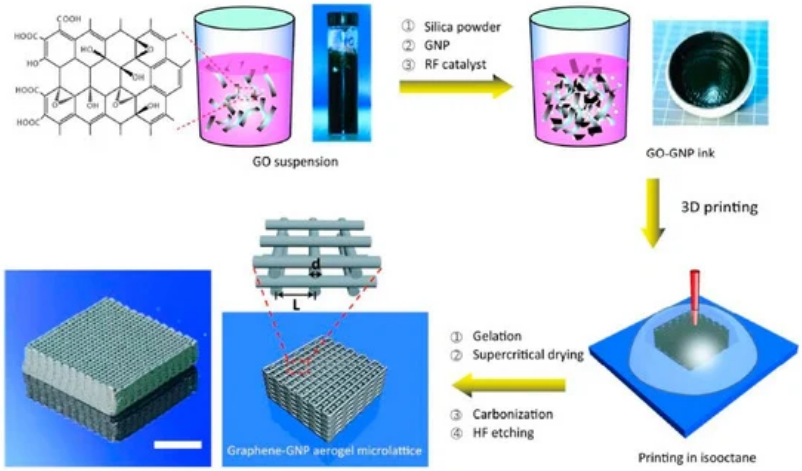

Figure 3. Schematic diagram part fabrication process: Mixing of SiO_2, GNPs and R-F with the aqueous GO suspension. Then, the as-prepared GO paste was extruded in an isooctane bath, and the as-obtained part was gelled at 85 °C, then dried using supercritical carbon dioxide. Finally, the silica fillers were etched using diluted hydrofluoric acid. The scale bar is 10 mm. Reprinted Reproduced from[43], with permission from American Chemical Society, 2016.

Another approach to preparing pastes with appropriate rheological properties for ceramic/graphene composites manufacturing by DIW could be the use of preceramic polymers (PCP)[44]. Preceramic polymers are polymeric compositions, particularly as organosilicon compounds (e.g., polymers based on a Si backbone containing N, O, H, C, and B atoms), which under pyrolysis at above ~800 °C in an atmosphere of argon or nitrogen are transformed into ceramic materials, also referred to as polymer derived ceramics (PDCs)[45]. With the addition of PCPs into the graphene-based feedstock is possible to alter the properties, structures and phase of the material after heat treatment.

Pierin et al. reported a method for the manufacturing of micro-sized SiOC ceramic components by DIW using a preceramic polymer[46]. The mixing of siloxane resin dissolved in a solvent with cross-linked preceramic grains ensured the appropriate rheological performance of pastes. Moreover, for improved the structural stability via pyrolysis the low amount (0.025–0.1 wt%) of GO was added to the paste formulation, resulting in reduced shrinkage of the preceramic polymer. The resulting parts after pyrolysis at 1000 °C showed an appropriate value of 2.5 MPa and 3.1 MPa of compression strength for a 64 vol% total porosity and after the addition of 0.1 wt% GO, respectively. Zhong et al. first developed GO/geopolymer (GOGP) nanocomposite structures fabricated by DIW, Figure 4 [39]. The authors noted that the addition of graphene oxide in the geo-polymeric water-based mixture (aluminosilicate and alkaline-source particles) intensely modifies its rheology behavior allowing the DIW which would not be possible solely by geo-polymer. Paste preparation involves the obtaining of geo-polymeric suspension by mixing of alkaline-source particles and aluminosilicates particles (ASOPs) in water. After stirring for 20 min, suspensions with diverse amounts of GO (4, 5, 10, and 20 wt%) were added into the as-prepared geo-polymeric suspension at a temperature below 5 °C. This low temperature avoids the geo-polymerization and the GO reduction that could happen at relatively high temperatures which in turn can lead to heterogeneous structure due to agglomeration of nanoparticles. When GO is added into geo-polymeric suspension, its rheological properties change dramatically. For the GOGP with 4 wt% of graphene oxide the storage (G′) and loss modulus (G″) increased to ~1 × 10^5 Pa and ~1.5 × 10^4 Pa (at the stress of 50 Pa, that is typically used in DIW) that are over one and two orders of magnitude higher than the values of storage (G′) and loss (G″) moduli of pure geopolymer, respectively. In addition, the yield stress of the GO-based geo-polymeric suspension is as high as ~2000 Pa. When the GO concentration increases up to 5 wt% of GO the yield stress decrease to ~1000 Pa, while the storage modulus

increased further. However, when the concentration of GO in nanocomposites increases above the range of 10, and 20 wt%, a decrease of the modulus is showed, which is probably associated with the lubrication effects of GO. The characterization of cured parts showed that GO nanosheets anchored themselves in geo-polymer and encapsulated individual geo-polymer grains, Figure 5 [39], in order to obtain a 3D network across the nanocomposites. The as-obtained cured parts showed high mechanical properties (compressive strength > 30 MPa), while after sintering at 1000 °C the parts achieved a conductivity of 10^2 S/m.

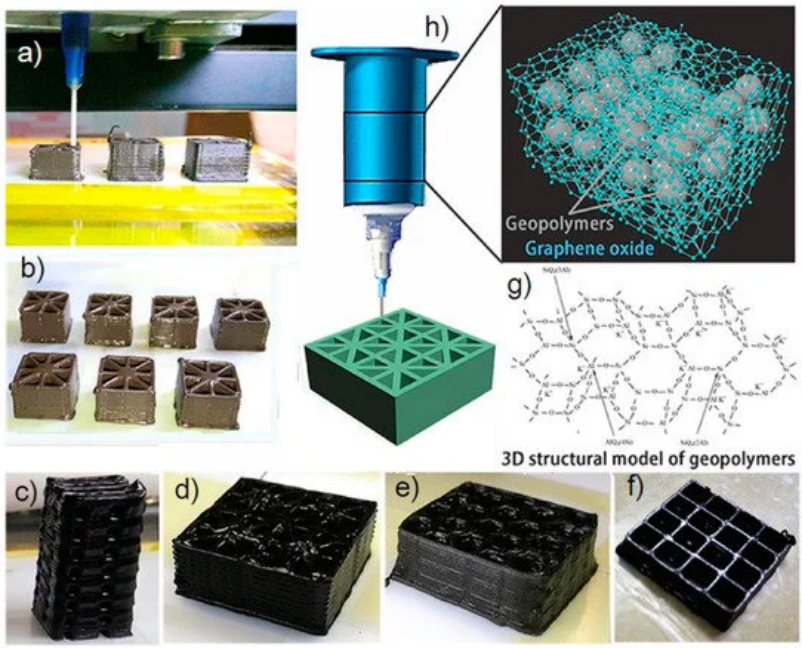

Figure 4. (**a**–**f**) 3D printing process and some 3D printed structures. (**b**–**f**) The colors of the printed samples turn from brownish to blackish when the GO loading increased. (**g**) The chemical structure of geopolymer, and (**h**) schematic diagrams of the painting process and the composite structure are also showed. Reproduced from[39], with permission from Elsevier, 2017.

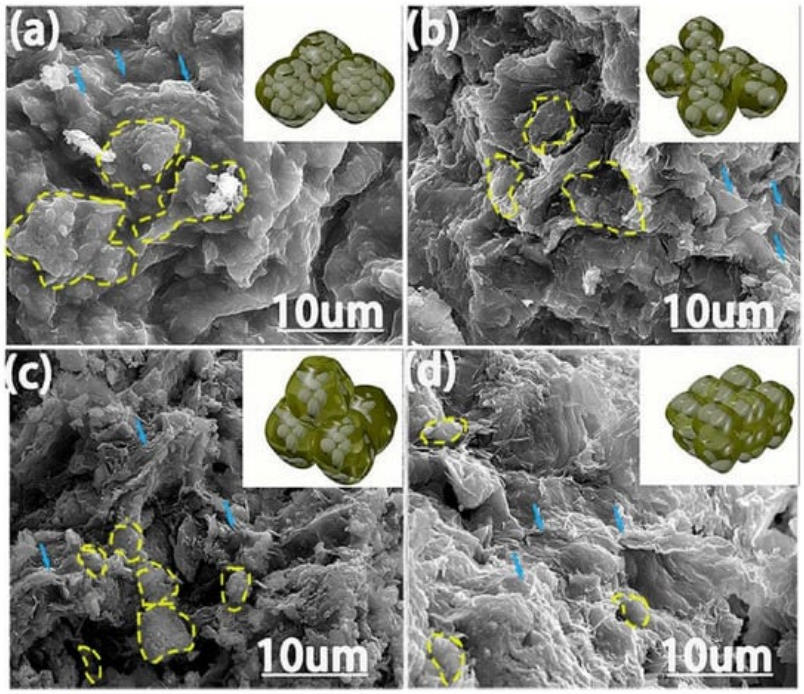

Figure 5. SEM images of hydrated geopolymer particles encapsulated by graphene oxides sheets (**a**–**d**), and their models. With the increase of GO concentration from 4 wt% to 20 wt% in nanocomposites, the agglomerate size (showed by dotted-line circles) decrease. Reproduced from[39], with permission from Elsevier, 2017.

In the state of the art of graphene-based ceramic 3D printed composites using preceramic polymers, interesting methods, which differ from the above examples in the way that ceramic phase is introduced in the 3D part, can be found. Commonly in these solutions, a 3D graphene-based part is first manufactured by DIW; then, it is heated for polymer removal followed by an infiltration step of a ceramic precursor[47][48][49].

Román-Manso et al. developed an approach to manufacture PDC/GO composites. In this low-temperature method, the first 3D structures were fabricated by DIW using an aqueous GO paste with polymeric additives. Then, the obtained graphene oxide periodic structures were dried in a drying furnace at ~80 °C and immediately afterward frozen in a refrigerator at −20 °C. This leads to prevent the formation of a network of evenly spaced cracks in the composites structure caused by the presence of water. Subsequently, the as-fabricated graphene oxide structures were lyophilized to sublimate the ice. Finally, in order to ensure the diffusion of the liquid into the structure rods, highly porous 3D structures were impregnated by immersion in a liquid organic-polysilazane (a compound of Si, C, H, N) during several hours. For crosslinking and pyrolysis these impregnated structures were placed on the Pt foil in alumina crucibles in a tubular electric furnace and heated at 200 °C and 800–1000 °C, respectively, in N_2 atmosphere. Figure 6a [47], shows the printed graphene oxide and pyrolyzed composite structure which has remained the shape retention and the high shrinkage.

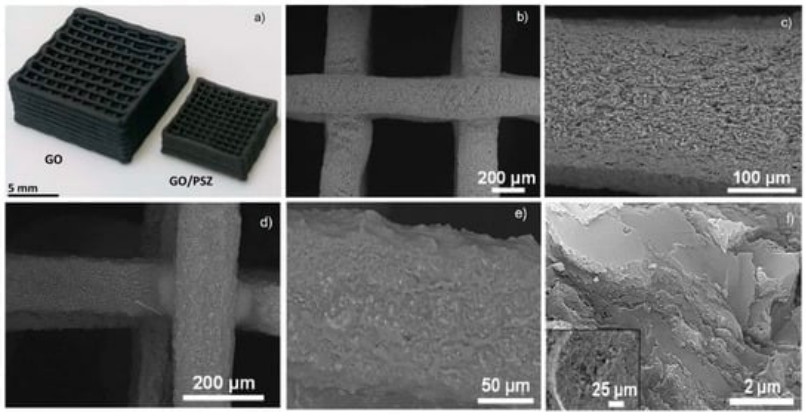

Figure 6. (**a**) 3D printed scaffolds of GO (as-printed) and the composite structure GO/PSZ pyrolyzed at 800 °C. SEM micrographs of a GO lattice after dying/lyophilization steps showing a top view (**b**) and the surface of an extruded filament (**c**). Analogous SEM images of a PSZ infiltrated GO lattice pyrolyzed at 800 °C in N_2, (**d**) top view, (**e**) filament and (**f**) cross-section at different magnifications. Reproduced from[47], with permission from Elsevier, 2018.

Figure 6b,c,[47], exhibits views from above of a sublimated GO structure at different magnifications. The linear shrinkage of the lattice was caused by quick-drying treatment.

Figure 6d–f,[47], show printed GO structures after the complete infiltration. No substantial cracking (Figure 6d,e,[47]) is detected in the infiltrated structures after pyrolysis (800–1000 °C). These PDC/GO composites imitate modeled graphene oxide skeleton and, while the conductive network (electrical conductivity in the range 0.2–4 S/cm) of the composite is provided by the presence of graphene. The ceramic coating serves as a protective barrier for the graphene network against the atmosphere, temperature (up to 900 °C in the air) and even direct flame.

Similar work was carried out by Moyano et al.[48], in which they studied the electrical, mechanical and capacitive responses of a strong and light 3D ceramic/graphene structure obtained through a controllable and fast infiltration method using a preceramic polymer.

Another interesting approach was reported by You et al.[49]. In this work, the authors proposed a method for the growth of SiC that it exactly occurs in 3D printed graphene scaffolds by means of chemical vapor infiltration (CVI). The structures were fabricated using the addition of graphene to ethylene glycol butylether (EGB) in ethanol, followed by sonication and addition of dibutyl phthalate (DBP) and polyvinyl butyral (PVB), resulting in homogeneous graphene-based suspension. Next, the ethanol was evaporated in a water bath at 80 °C with continuous stirring. The as-prepared suspension had a graphene concentration of 200 mg/mL. After, the graphene scaffolds were printed using the as-prepared paste. Subsequently, the printed objects were located in the Ar flow through a carbon tube furnace and heated to 1100 °C for thermal decomposition of organic-polymer. The polymer decomposition allows a large specific surface area of the scaffold that has a positive effect on the densification and the in-situ growth of the SiC. Thus, the SiC matrix was introduced into the pores of the 3D graphene scaffold by cracking methyltrichlorosilane (MTS) in the CVI process. The concentration and structure of the SiC in the composite were monitored by adjusting the holding time and gas pressure, which are the main CVI parameters.

Finally, the 3D graphene/SiC composites show enhanced mechanical properties, especially compressive strength (193 ± 15.7 MPa) which is 394% higher compared to directly mixed products. Besides, the reconciling of the 3D graphene structure and SiC matrix produces a huge number of conductive paths and gives a composite improved electrical conductivity compared to traditional ceramic materials.

Unfortunately, in these last three examples, it is not possible to directly obtain a 3D printed part from which a graphene-based/ceramic composite is obtained after sintering. In these examples, an additional step of ceramic material infiltration into the graphene skeleton is necessary.

As we have seen in this section, each of the discussed methods includes a preparing step of the graphene-based paste that requires at least the presence of an additive, which is mainly utilized to guarantee a homogeneous dispersion and to achieve the suitable viscoelastic properties. In the majority of cases, the additives are eliminated either by a chemical etching or a thermal process at high temperatures, which causes the appearance of pores in its structure that can negatively influence the composite mechanical properties.

In recent years, attempts have been made to find new methods to minimize the presence of additives in graphene-based paste formulations for DIW. For example, García-Tuñón et al. developed a clean, flexible and robust approach to formulating pastes used in DIW that can be adapted to a wide range of materials[29]. Thus, they prepared free additive pastes of diverse materials (polymer, ceramic and metal), based only on the use of GO as the dispersant, rheological modifier, and binder. This procedure was possible to realize thanks to the great similarities between GO and clay. These materials have a flake-like shape with oxygen-containing functional groups on their basal planes and the edges that promote the network connection between particles thanks to the electrostatic and noncovalent interactions for clay and GO respectively. Clay has exceptional chemistry and structure that permit the design of water-based suspensions for shaping with excellent viscoelastic behavior. For this reason, it is added to ceramics suspensions to reach the required viscoelastic behavior for processing. On the other hand, as for clay, the especial combination of GO sheets surface chemistry and structure in contact with water under special conditions allow the preparation of a very stable GO paste with proper viscoelastic behavior for different materials with have a broad variety of particle morphologies, sizes, and chemistries. In this research, various kinds of graphene-based paste with ceramic (Al_2O_3 powders and platelets, SiC powders) were prepared and, then, used for the printing of ceramic parts. The increases of the paste concentration were reached by two different approaches: 1–redispersing freeze-dried GO powders and 2–by evaporation of water at 70 °C. In the two cases, pastes with a high concentration of GO and the necessary viscoelastic behavior for printing were obtained without the addition of any additive. Furthermore, in some cases of the paste preparations, certain amounts of freeze-dried GO powder were added in order to achieve the necessary characteristics of viscoelasticity and flow. Finally, the pastes prepared in this work were formed as indicated below: (1) 28.4 vol% SiC with 0.4 vol% GO (10 mg/mL), (2) 23 vol% Al_2O_3 platelets (0.8 vol% GO (23 mg/mL)) and (3) 27 vol% Al_2O_3 platelets (1.1 vol% GO (33 mg/mL)).

The authors found that GO suspensions with a concentration above ~2 vol% showed an increase of the storage modulus (G′, Figure 7a,b,[29]) as a result of a well-established and organized formed structure in them (Figure 7d,[29]). The reorganization of the GO flakes occurs when the concentration of the suspension increases thus creating a network like a liquid crystal, which produces growth of the storage modulus (G′) up to 100 kPa (Figure 7b,[29]) and the yield stress up to 2300 Pa (Figure 7c,[29]). Besides, the GO pastes with concentrations from 2.5 to 3.5 vol% have the necessary structure and rheological properties for DIW (labeled 3D-printable in Figure 7a,[29]).

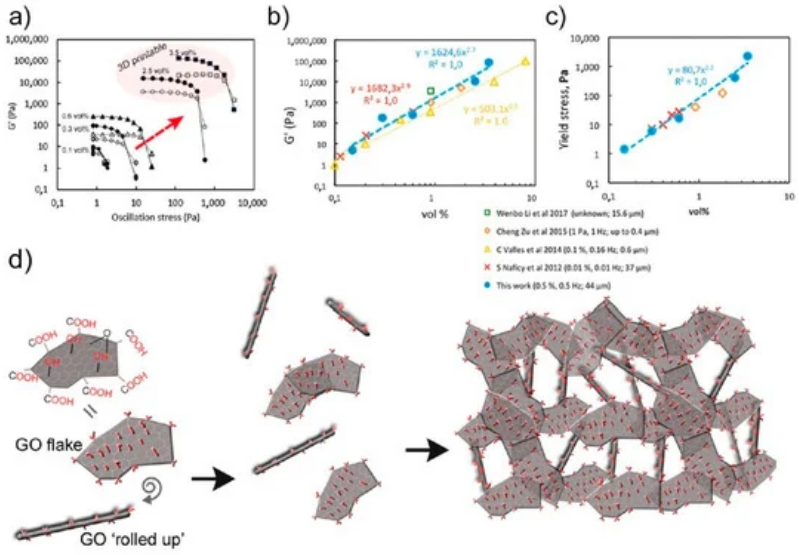

Figure 7. Viscoelastic behavior of pastes and GO suspensions: Storage Modulus (G′) vs. Oscillation Stress (**a**), and GO concentration influence on G′ (**b**), and yield stress (**c**). The proposed network created by GO flakes as concentration increases (**d**). A part of GO sheets form GO scrolls that together with the sheets bring together forming a 3D liquid crystal structure with high G′ (**a**). Reproduced from[29], with permission from American Chemical Society, 2017.

For the Al_2O_3 platelets pastes, the concentration of 1.1 vol% GO and ~28 vol% platelets showed the greatest behavior for printing (Figure 8,[29]). During extrusion an orientation of platelets and an internal structure formation of printed filaments took place. The FESEM images of printed filament cross-section and lateral view are shown in Figure 8c,d,[29]) respectively. In them is possible to see how the platelets form a wall on the outside edge (Figure 8d,[29]), while the filament inside part has a mixture of domains (Figure 8c,[29]). A more detailed observation demonstrated that GO sheets are distributed over and across multiple Al_2O_3 platelets interacting with a very strong form, binding them together and forming bridges across them. After sintering, the structures made with GO had an average porosity of 60% with only 2% closed pores and showed good handling strength, Figure 9 [29].

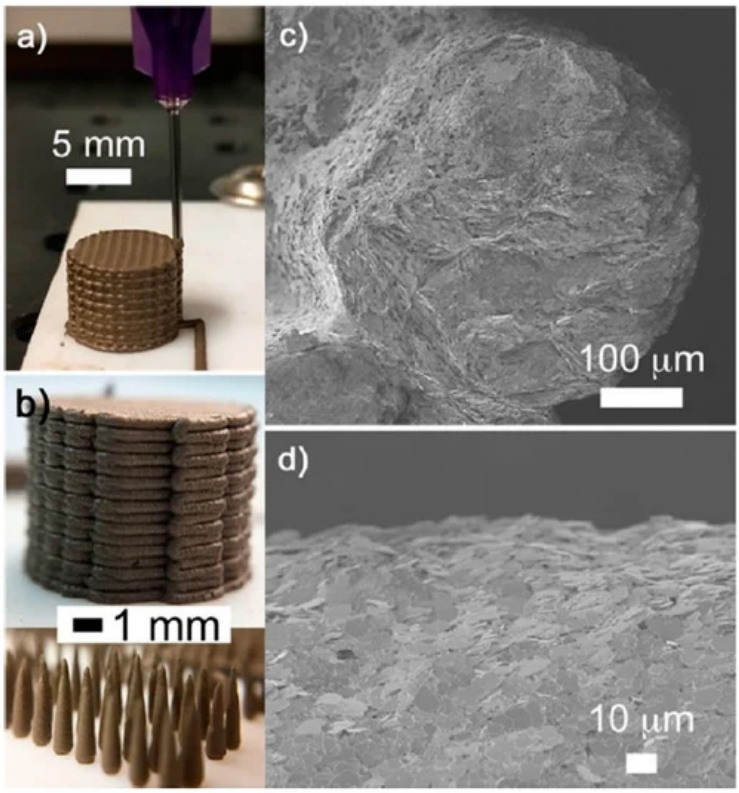

Figure 8. Printed objects from GO/Al_2O_3 platelets paste (**a**,**b**) and cross-section and lateral view of printed filament (**c**,**d**). Reproduced from[29], with permission from American Chemical Society, 2017.

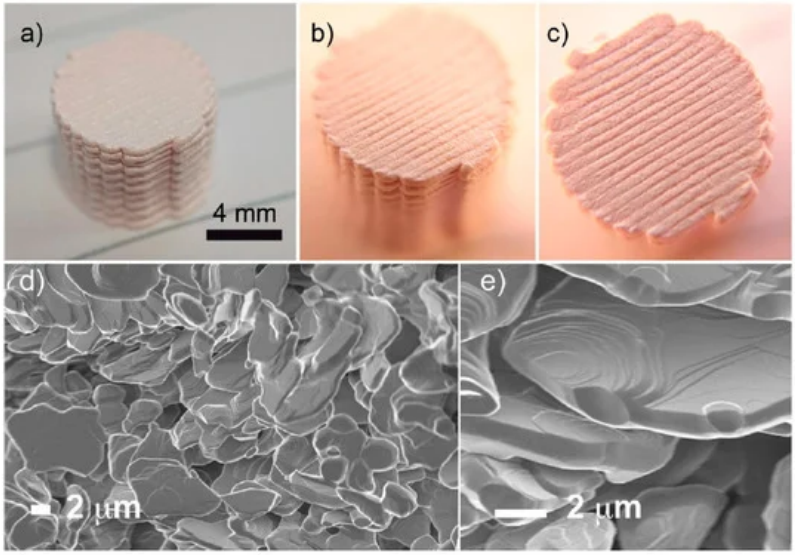

Figure 9. Cylinder printed by DIW from GO/Al_2O_3 platelets paste and sintered at 1550 °C. (**a**–**c**). The SEM images show the cylinder microstructure with open porosity of 60% determined by Archimedes' Principle (**d**,**e**). Reproduced from[29], with permission from American Chemical Society, 2017.

The SiC paste also showed suitable printing behavior. Dried 3D printed bars had strengths of ~1 MPa which demonstrates that in this case the GO also operates as a binding agent between the SiC particles. Bars printed from GO/SiC paste and sintered at 2050 °C for 2 h showed a density of 3.21 g/cm^3 and reached a bending strength of around 212 MPa.

In both cases, Al_2O_3 and SiC were the unique crystalline phase in the sintered objects, and Raman spectroscopy demonstrated that no carbon residues remained in the structure. Note that, it is possible to add potentially structural or functional properties to the sintered 3D object simply retaining the GO in the structure after sintering.

Summarizing, this method permits us to form complex 3D ceramic structures using DIW, which have properties that are similar to alternative formulations, and demonstrates the possibility of using 2D colloids in materials manufacturing.

3. Summary

In this article, it was shown that significant advances in additive technologies for 3D printing of graphene-based ceramic composites have been made in recent years. The state of the art of different additive techniques used for the manufacturing of both ceramic and graphene-based pieces was analyzed. In addition, various examples of 3D printing of graphene-based ceramic composites were discussed.

First, a summary of existing additive technologies groups, techniques that are involved with them, and of the most popular feedstock nowadays was made, (see Table 1). After that, it was clear that not all additive manufacturing (AM) technologies apply to the ceramic part manufacturing and even more for the graphene-based materials.

The introduction of Additive Manufacturing to the production of ceramics is related to the need to obtain complex parts that are not possible to produce using conventional methods since 3D printing can manufacture complex structures in a fast, simple and inexpensive way.

Second, the state of the art of Direct ink writting (DIW), which is a AM technology that use a pseudo-plastic feedstock (paste) for the fabrication of 3D printed parts, has been considered and demonstrated with symbolic examples. In this section, it was demonstrated that DIW is the most studied technique and one of the most widely used for the manufacture of 3D parts from a graphene-based feedstock thanks to the combination of the great possibilities of this technique with the unique properties of graphene, which has showed remarkable printing capabilities with unique viscoelastic properties. Moreover, it was explained that the formulation of suitable graphene-based feedstocks is possible by the use of graphene oxide, the main precursor of graphene, because it can be easily dispersed in water and other solvents, which is not possible with pristine graphene. It is emphasized that in DIW the graphene-based feedstock rheological behavior plays a very important role, and it is essential to establish the appropriate content of the feedstock components to obtain their homogeneous dispersion and the appropiate viscoelastic property.

Additionally, some examples of printed composites from graphene-based ceramic pastes by DIW is carried out. In this field, there is a tendency to reduce the number of additives that are used for obtaining a homogeneous dispersion and very often produce undesired effects. Some examples show that it is possible the use preceramic polymers for the reduction of additives and to perform the characteristics of printed composites. Of great importance is the work carried out to create ceramic pastes without any other additives than graphene oxide. Here it is appreciated how this material can be used as a dispersant, rheological modifier and binder at the same time.

This work has tried to show that the DIW method is very promising in the printing of complex graphene-based ceramic composites at reduced cost and in less time . We consider that this field should continue to develop so that soon the manufacture of graphene-based ceramic composites will take its place in the ceramic industry.

Funding: We would like to thank the Russian Science Foundation for supporting this work under grant 19-79-00355.

References

1. Kingery, W.D.; Bowen, H.K.; Uhlmann, D.R. . Introduction to Ceramics, 2nd ed.; Wiley: New York, NY, USA, 1976; pp. 1–1056.
2. Carter, C.B.; Norton, M.G. . Ceramic Materials: Science and Engineering; Springer: New York, NY, USA, 2013; pp. 1–766.
3. Smirnov, A.; Kurland, H.-D.; Grabow, J.; Müller, F.A.; Bartolomé, J.F. Microstructure, mechanical properties and low temperature degradation resistance of 2Y-TZP ceramic materials derived from nanopowders prepared by laser vaporization. J. Eur. Ceram. Soc. 2015, 35, 2685–2691.
4. Smirnov, A.; Beltrán, J.I.; Rodriguez-Suarez, T.; Pecharromán, C.; Muñoz, M.C.; Moya, J.S.; Bartolomé, J.F. Unprecedented simultaneous enhancement in flaw tolerance and fatigue resistance of zirconia–Ta composites. Sci. Rep. 2017, 7, 44922.
5. Smirnov, A.; Bartolomé, J.F.; Kurland, H.-D.; Grabow, J.; Müller, F.A. Design of a new zirconia-alumina-Ta micro-nanocomposite with unique mechanical properties. J. Am. Ceram. Soc. 2016, 99, 3205–3209.
6. Bartolomé, J.F.; Smirnov, A.; Kurland, H.-D.; Grabow, J.; Müller, F.A. New ZrO2/Al2O3 nanocomposites fabricated from hybrid nanoparticles prepared by CO2 laser Co-vaporisation. Sci. Rep. 2016, 6, 20589.
7. Smirnov, A.; Bartolomé, J.F. Microstructure and mechanical properties of ZrO2 ceramics toughened by 5–20 vol% ta metallic particles fabricated by pressureless sintering. Ceram. Int. 2014, 40, 1829–1834.
8. Gutierrez-Gonzalez, C.F.; Smirnov, A.; Bartolomé, J.F. Cyclic fatigue life- and crack-growth behavior of zirconia-niobium composites. J. Am. Ceram. Soc. 2013, 96, 1709–1712.
9. Bengisu, M. Engineering Ceramics; Springer-Verlag: Berlin/Heidelberg, Germany, 2001; pp. 620.
10. Richerson, D.W.; Lee, W.E. Modern Ceramic Engineering: Properties, Processing, and Use in Design, 4th ed.; CRC Press: Boca, FL, USA, 2018; pp. 1–791.
11. Pristinskiy, Y.; Solis Pinargote, N.W.; Smirnov, A. The effect of MgO addition on the microstructure and mechanical properties of alumina ceramic obtained by spark plasma sintering. Mater. Today Proc. 2019, 19, 1990–1993.
12. Chen, Z.; Li, Z.; Li, J.; Liu, C.; Lao, C.; Fu, Y.; Liu, C.; Li, Y.; Wang, P.; He, Y. 3D printing of ceramics: A review. J. Eur. Ceram. Soc. 2019, 39, 661–687.
13. Abdulhameed, O.; Al-Ahmari, A.; Ameen, W.; Mian, S.H. Additive manufacturing: Challenges, trends, and applications. Adv. Mech. Eng. 2019, 11, 1–27.
14. Gibson, I.; Rosen, D.; Stucker, B. Additive Manufacturing Technologies: 3D Printing, Rapid Prototyping, and Direct Digital Manufacturing, 2nd ed.; Springer: New York, NY, USA, 2015; pp. 1–498.
15. International Organization for Standardization. ISO/ASTM 52900:2015 [ASTM F2792] Additive Manufacturing—General Principles—Terminology; ISO: Geneva, Switzerland, 2015.
16. Diegel, O. A Practical Guide to Design for Additive Manufacturing; Series in Advanced Manufacturing; Springer: New York, NY, USA, 2020; pp. 226.
17. Coppola, S.; Nasti, G.; Vespini, V.; Ferraro, P. Layered 3D printing by tethered pyro-electrospinning. Adv. Polym. Technol. 2020, 2, 1–9.

18. Coppola, S.; Vespini, V.; Nasti, G.; Gennari, O.; Grilli, S.; Ventre, M.; Iannone, M.; Netti, P.A.; Ferraro, P. Tethered pyro-electrohydrodynamic spinning for patterning well-ordered structures at micro- and nanoscale. Chem. Mater. 2014, 26, 3357–3360.
19. Coppola, S.; Nasti, G.; Todino, M.; Olivieri, F.; Vespini, V.; Ferraro, P. Direct writing of microfluidic footpaths by pyro-EHD printing. ACS Appl. Mater. Int. 2017, 9, 16488–16494.
20. Lewis, J.A.; Gratson, G.M. Direct writing in three dimensions. Mater. Today 2004, 7, 32–39.
21. Martínez-Vázquez, F.J.; Perera, F.H.; Miranda, P.; Pajares, A.; Guiberteau, F. Improving the compressive strength of bioceramic robocast scaffolds by polymer infiltration. Acta Biomater. 2010, 6, 4361–4368.
22. Lewis, J.A. Direct ink writing of 3D functional materials. Adv. Funct. Mater. 2006, 16, 2193–2204.
23. Revelo, C.F.; Colorado, H.A. 3D printing of kaolinite clay ceramics using the Direct Ink Writing (DIW) technique. Ceram. Int. 2018, 44, 5673–5682.
24. Martínez-Vázquez, F.J.; Pajares, A.; Miranda, P. A simple graphite-based support material for robocasting of ceramic parts. J. Eur. Ceram. Soc. 2018, 38, 2247–2250.
25. Ordoñez, E.; Gallego, J.M.; Colorado, H.A. 3D printing via the direct ink writing technique of ceramic pastes from typical formulations used in traditional ceramics industry. Appl. Clay Sci. 2019, 182, 105285.
26. Ahn, B.Y.; Duoss, E.B.; Motala, M.J.; Guo, X.; Park, S.I.; Xiong, Y.; Yoon, J.; Nuzzo, R.G.; Rogers, J.A.; Lewis, J.A. Omnidirectional printing of flexible, stretchable, and spanning silver microelectrodes. Science 2009, 323, 1590−1593.
27. Liu, D.-M. Influence of porosity and pore size on the compressive strength of porous hydroxyapatite ceramic. Ceram. Int. 1997, 23, 135–139.
28. Yao, Y.; Fu, K.K.; Yan, C.; Dai, J.; Chen, Y.;Wang, Y.; Zhang, B.; Hitz, E.; Hu, L. Three-dimensional printable high-temperature and high-rate heaters. ACS Nano 2016, 10, 272–5279.
29. García-Tuñón, E.; Feilden, E.; Zheng, H.; D'Elia, E.; Leong, A.; Saiz, E. Graphene oxide: An all-in-one processing additive for 3D printing. ACS Appl. Mater. Interfaces 2017, 9, 32977–32989.
30. Lewis, J.A. Colloidal processing of ceramics. J. Am. Ceram. Soc. 2000, 83, 2341−2359.
31. Xu, Z.; Gao, C. Aqueous liquid crystals of graphene oxide. ACS Nano 2011, 5, 2908−2915.
32. Solis Pinargote, N.W.; Peretyagin, P.; Torrecillas, R.; Fernández, A.; Menéndez, J.L.; Mallada, C.; Díaz, L.A.; Moya, J.S. Electrically conductor black zirconia ceramic by SPS using graphene oxide. J. Electroceram 2017, 38, 119–124.
33. Smirnov, A.; Peretyagin, P.; Bartolomé, J.F. Processing and mechanical properties of new hierarchical metal-graphene flakes reinforced ceramic matrix composites. J. Eur. Ceram. Soc. 2019, 39, 3491–3497.
34. Gutierrez-Gonzalez, C.F.; Smirnov, A.; Centeno, A.; Fernández, A.; Alonso, B.; Rocha, V.G.; Torrecillas, R.; Zurutuza, A.; Bartolomé, J.F. Wear behavior of graphene/alumina nanocomposite. Ceram. Int. 2015, 41, 7434–7438.
35. Cascales, A.; Tabares, N.; Bartolomé, J.F.; Cerpa, A.; Smirnov, A.; Moreno, R.; Nieto, M.I. Processing and mechanical properties of mullite and mullite–alumina composites reinforced with carbon nanofibers. J. Eur. Ceram. Soc. 2015, 35, 3613–3621.
36. Huang, C.-T.; Kumar Shrestha, L.; Ariga, K.; Hsu, S.-H. A graphene-polyurethane composite hydrogel as a potential bioink for 3D bioprinting and differentiation of neural stem cells. J. Mater. Chem. B 2017, 5, 8854–8864.
37. Wang, J.; Liu, Y.; Fan, Z.; Wang, W.; Wang, B.; Guo, Z. Ink-based 3D printing technologies for graphene-based materials a review. Adv. Compos. Hybrid Mater. 2019, 2, 1–33.
38. Roman-Manso, B.; Figueiredo, F.M.; Achiaga, B.; Barea, R.; Perez-Coll, D.; Morelos-Gomez, A.; Terrones, M.; Osendi, M.I.; Belmonte, M.; Miranzo, P. Electrically functional 3D-architectured graphene-SiC composites. Carbon 2016, 100, 318–328.
39. Zhong, J.; Zhou, G.-X.; He, P.-G.; Yang, Z.-H.; Jia, D.-C. 3D printing strong and conductive geo-polymer nanocomposite structures modified by graphene oxide. Carbon 2017, 117, 421–426.
40. Tubio, C.R.; Rama, A.; Gomez, M.; del Rio, F.; Guitian, F.; Gil, A. 3D-printed graphene-Al2O3 composites with complex mesoscale architecture. Ceram. Int. 2018, 44, 5760–5767.
41. Moyano, J.J.; Gomez-Gomez, A.; Perez-Coll, D.; Belmonte, M.; Miranzo, P.; Osendi, M.I. Filament printing of graphene-based inks into self-supported 3D architectures. Carbon 2019, 151, 94–102.
42. de la Osa, G.; Perez-Coll, D.; Miranzo, P.; Osendi, M.I.; Belmonte, M. Printing of graphene nanoplatelets into highly electrically conductive three-dimensional porous macrostructures. Chem. Mater. 2016, 28, 6321–6328.

43. Zhu, C.; Liu, T.; Qian, F.; Han, T.Y.-J.; Duoss, E.B.; Kuntz, J.D.; Spadaccini, C.M.; Worsley, M.A.; Li, Y. Supercapacitors based on three-dimensional hierarchical graphene aerogels with periodic macropores. Nano Lett. 2016, 16, 3448–3456.
44. Shen, C.; Calderon, J.E.; Barrios, E.; Soliman, M.; Khater, A.; Jeyaranjan, A.; Tetard, L.; Gordon, A.; Seal, S.; Zhai, L. Anisotropic electrical conductivity in polymer derived ceramics induced by graphene aerogels. J. Mater.Chem. C 2017, 5, 11708–11716.
45. Bernardo, E.; Fiocco, L.; Parcianello, G.; Storti, E.; Colombo, P. Advanced ceramics from preceramic polymers modified at the nano-scale-a review. Materials 2014, 7, 1927–1956.
46. Pierin, G.; Grotta, C.; Colombo, P.; Mattevi, C. Direct Ink Writing of micrometric SiOC ceramic structures using a preceramic polymer. J. Eur. Ceram. Soc. 2016, 36, 1589–1594.
47. Manso, B.R.; Moyano, J.J.; Perez-Coll, D.; Belmonte, M.; Miranzo, P.; Osendi, M.I. Polymer-derived ceramic-graphene oxide architected composite with high electrical conductivity and enhanced thermal resistance. J. Eur. Ceram. Soc. 2018, 38, 2265–2271.
48. Moyano, J.J.; Mosa, J.; Aparicio, M.; Pérez-Coll, D.; Belmonte, M.; Miranzo, P.; Osendi, M.I. Strong and light cellular silicon carbonitride–Reduced graphene oxide material with enhanced electrical conductivity and capacitive response. Addit. Manuf. 2019, 30, 100849.
49. You, X.; Yang, J.; Huang, K.; Wang, M.; Zhang, X.; Dong, S. Multifunctional silicon carbide matrix composites optimized by three-dimensional graphene scaffolds. Carbon 2019, 155, 215–222.
